

**Fig. 4.** FKHRL1 regulates hydrogen peroxide scavenging and oxidative stress resistance. (A) FKHRL1 stimulated transcriptional activity using a catalase promoter beginning at  $-3179$  (black bar) or at  $-1645$  (striped bar) or with a synthetic promoter containing three tandem forkhead binding sites (stippled bar). Transcriptional activity was determined after transfection with increasing amounts of either full-length FKHRL1 (WT) or the activation domain deficient FKHRL1 mutant ( $\Delta C$ ) isoform (8). (B) Total hydrogen peroxide scavenging capacity in control cells (Neo), cell stably expressing the activation deficient FKHRL1 mutant ( $\Delta C$ ) or cells expressing full-length FKHRL1 (WT). (C) Cell survival in PC12 cell lines 24 hours after exposure to hydrogen peroxide ( $200 \mu\text{M}$ ).

creased survival after direct hydrogen peroxide challenge (Fig. 4C).

Our results, therefore, demonstrate an important functional relation between forkhead proteins that regulate longevity in *C. elegans*, *p66shc* that is implicated in mammalian life span, and intracellular oxidants, which are thought to play a role in aging across all species (1). We have also demonstrated a role for FKHRL1 expression in the regulation of cellular oxidative stress resistance. This is consistent with previous studies demonstrating that DAF-16 can act as a potential transcriptional activator of several antioxidant scavengers and stress resistance genes in *C. elegans* including superoxide dismutase (SOD), catalase, and OLD-1 (2, 12–14). In contrast, most evidence in mammalian cells to date suggests that, after trophic withdrawal, transient activation of forkhead proteins is associated with increased cell death (3, 17, 18). Similarly, a number of studies have indicated a potentially protective effect of Akt activation after exposure to hydrogen peroxide (19–22). These observed differences in the protective versus harmful effects of Akt and forkhead proteins may relate to the levels of activation seen in these various studies, the nature of stimulus used, the differences between transient and stable FKHRL1 overexpression, or differences in the cell lines used. Whereas small increases in DAF-16 activity are associated with longevity in *C. elegans*, more robust activation results in a dauer-like state characterized by growth arrest (9, 23). In mammalian cells, although increased forkhead activity can be associated with cell death, inhibiting forkhead activity can also result in apoptosis (24).

Lastly, since the initial description over 40 years ago of the free radical theory of aging (25) the implication has been that ROS act solely as random, destructive agents. The

observation that forkhead activity is regulated by intracellular ROS in a *p66shc*-dependent fashion suggests that intracellular hydrogen peroxide might also provide a specific signaling function. Given that oxidative stress has been implicated in a host of human diseases as well as human aging, this expanded role for ROS as signaling agents may have important therapeutic implications.

**References and Notes**

1. T. Finkel, N. J. Holbrook, *Nature* **408**, 239 (2000).
2. J. Taub *et al.*, *Nature* **399**, 162 (1999).
3. A. Brunet *et al.*, *Cell* **96**, 857 (1999).

4. E. D. Tang, G. Nuñez, F. G. Barr, K. L. Guan, *J. Biol. Chem.* **274**, 16741 (1999).
5. W. H. Biggs *et al.*, *Proc. Natl. Acad. Sci. U.S.A.* **96**, 7421 (1999).
6. G. J. P. L. Kops *et al.*, *Nature* **398**, 630 (1999).
7. H. Takaiishi *et al.*, *Proc. Natl. Acad. Sci. U.S.A.* **96**, 11836 (1999).
8. Supplemental materials are available on Science Online at [www.sciencemag.org/cgi/content/full/1069004/DC1](http://www.sciencemag.org/cgi/content/full/1069004/DC1).
9. S. T. Henderson, T. E. Johnson, *Curr. Biol.* **11**, 1975 (2001).
10. E. Migliaccio *et al.*, *Nature* **402**, 309 (1999).
11. S. Nemoto, unpublished observations.
12. Y. Honda, S. Honda, *FASEB J.* **13**, 1385 (1999).
13. D. Barsyte, D. A. Lovejoy, G. J. Lithgow, *FASEB J.* **15**, 627 (2001).
14. S. Murakami, T. E. Johnson, *Curr. Biol.* **11**, 1517 (2001).
15. T. Furuyama, T. Nakazawa, I. Nakano, N. Mori, *Biochem. J.* **349**, 629 (2000).
16. R. H. Medema, G. J. P. L. Kops, J. L. Bos, B. M. T. Bugnering, *Nature* **404**, 782 (2000).
17. W. H. Zheng, S. Kar, R. Quirion, *J. Biol. Chem.* **275**, 39152 (2000).
18. A. Brunet *et al.*, *Mol. Cell. Biol.* **21**, 952 (2001).
19. Y. Sonoda *et al.*, *J. Biol. Chem.* **274**, 10566 (1999).
20. H. Hang *et al.*, *J. Biol. Chem.* **276**, 26357 (2001).
21. X.-T. Wang *et al.*, *J. Biol. Chem.* **276**, 28364 (2001).
22. M. Salinas, D. Martin, A. Alvarez, A. Cuadrado *Mol. Cell. Neurosci.* **17**, 67 (2001).
23. R. Y. N. Yee, J. Hench, G. Ruvkun, *Curr. Biol.* **11**, 1950 (2001).
24. H. Leenders, S. Whitfield, S. Benoist, D. Mathis, *Eur. J. Immunol.* **30**, 2980 (2000).
25. D. Harman, *J. Gerontol.* **2**, 298 (1957).
26. We wish to thank M. Greenberg, Y. Luo, S. G. Rhee, L. Lanfranco, and P. G. Pellicci for reagents; S. Gutkind for helpful discussions; and I. Rovira for help with the manuscript and figures. We are particularly grateful for the help of N. J. Holbrook and X. Wang.

14 December 2001; accepted 22 February 2002  
 Published online 7 March 2002;  
[10.1126/science.1069004](http://10.1126/science.1069004)  
 Include this information when citing this paper.

## Visualization of a Ran-GTP Gradient in Interphase and Mitotic *Xenopus* Egg Extracts

Petr Kalab, Karsten Weis,\* Rebecca Heald\*

The small guanosine triphosphatase Ran is loaded with guanosine triphosphate (GTP) by the chromatin-bound guanine nucleotide exchange factor RCC1 and releases import cargoes in the nucleus during interphase. In mitosis, Ran-GTP promotes spindle assembly around chromosomes by locally discharging cargoes that regulate microtubule dynamics and organization. We used fluorescence resonance energy transfer-based biosensors to visualize gradients of Ran-GTP and liberated cargoes around chromosomes in mitotic *Xenopus* egg extracts. Both gradients were required to assemble and maintain spindle structure. During interphase, Ran-GTP was highly enriched in the nucleoplasm, and a steep concentration difference between nuclear and cytoplasmic Ran-GTP was established, providing evidence for a Ran-GTP gradient surrounding chromosomes throughout the cell cycle.

Because of the chromosomal localization of the Ran-guanine nucleotide exchange factor (GEF) RCC1 (regulator of chromosome condensation 1) and the cytoplasmic localization of Ran-GAP (Ran-guanosine triphospha-

tase-activating protein) and its cofactor Ran-BP1 (Ran-binding protein 1), Ran-GTP is predicted to exist exclusively in the interphase nucleus or in the immediate proximity of mitotic chromosomes, whereas the bulk of

REPORTS

cytoplasmic Ran is rapidly converted to its guanosine diphosphate (GDP)-bound form (1). During interphase, the Ran cycle regulates the binding and release of transport cargoes from their receptors in the nucleus or cytoplasm, giving directionality to nucleocytoplasmic transport (2, 3). A Ran-GTP gradient is also proposed to regulate spindle formation during mitosis (4, 5), because Ran-GTP modulates microtubule dynamics and organization (4–8). In addition, Ran appears to regulate nuclear envelope reassembly upon exit from mitosis (9, 10). Recently, the nuclear import receptor importin  $\beta$  has been identified as a key factor regulated by Ran-GTP during spindle morphogenesis (11–13). Importin  $\beta$  acts as an inhibitor of spindle assembly and is thought to function by sequestering cargoes required for microtubule polymerization and organization. Ran-GTP generated in the vicinity of chromosomes binds importin  $\beta$  and discharges these cargoes. However, the existence of a Ran-GTP gradient during interphase or mitosis has remained hypothetical, and although several lines of evidence support this model, it has never been demonstrated experimentally.

Based on Ran's binding partners and regulation of nuclear transport factor-cargo interactions, we designed two chimeric biosensor probes that exhibit intramolecular fluorescence resonance energy transfer (FRET) between cyan fluorescent protein (CFP) and yellow fluorescent protein (YFP), modulated by the Ran nucleotide state (Fig. 1A) (14). In the absence of binding partners, we predicted that probe flexibility should allow FRET caused by the transfer of energy from a COOH-terminal CFP to an NH<sub>2</sub>-terminal YFP, leading to a decrease of CFP (donor) emission and an increase of YFP (acceptor) emission (15). The first sensor, designed to monitor the Ran nucleotide state directly, contained the Ran-binding domain (RBD) of the yeast Ran-GAP accessory factor Yrb1 (16). The RBD has a low affinity for Ran-GDP but binds to Ran-GTP in an extended conformation with its NH<sub>2</sub>- and COOH-termini ~5.6 nm apart (17). Thus, the YFP-RBD-CFP chimera (YRC) should not undergo FRET in the presence of Ran-GTP (Fig. 1A).

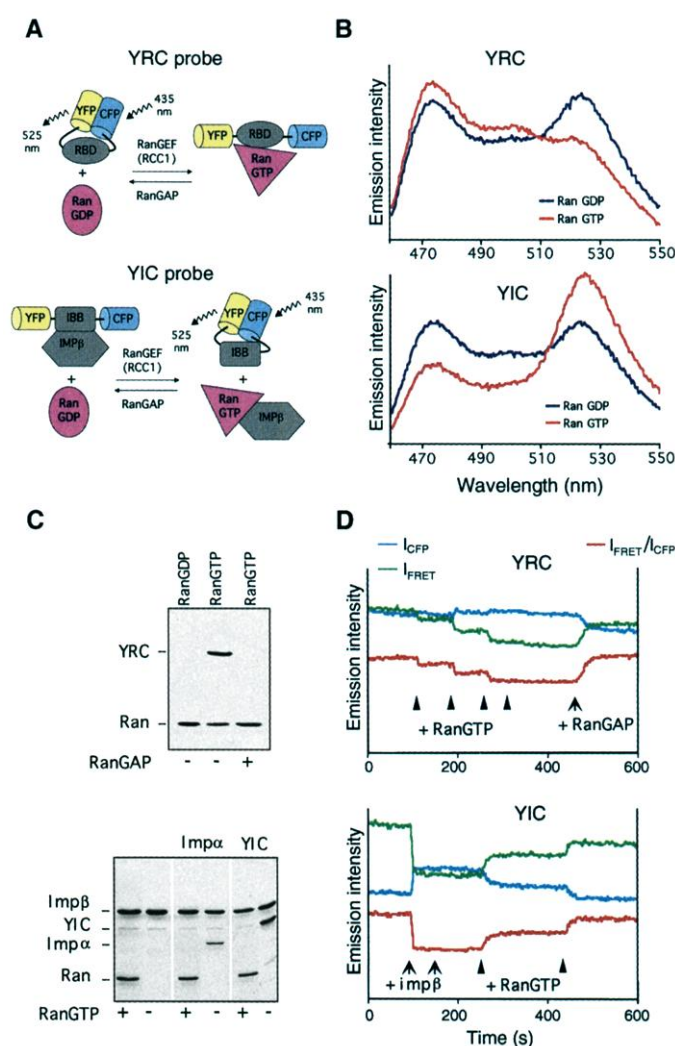
The second sensor was designed to monitor the release of importin  $\beta$  cargoes, which is regulated by the local concentration of Ran-GTP. We used the importin  $\beta$ -binding domain (IBB) of importin  $\alpha$  as a model cargo. Importin  $\alpha$  acts as an adapter to bind a subset of nuclear cargoes and is dissociated from importin  $\beta$  by Ran-GTP

(18–20). The free IBB domain is highly flexible (21), and the YFP-IBB-CFP (YIC) chimera should undergo FRET. However, when bound to importin  $\beta$ , the IBB forms an  $\alpha$ -helical rod ~5 nm long (22), and FRET of the YIC sensor should be inhibited (Fig. 1A). Thus, this probe should directly monitor free importin  $\beta$  cargoes and provide an indirect measure of Ran-GTP concentration.

To characterize the behavior of the YRC and YIC chimeras, their emission profiles were examined by spectrofluorimetry with 435-nm excitation in the presence of either Ran-GDP or Ran-GTP (Fig. 1B) (23). Under opposite Ran nucleotide states, the two

probes displayed an emission increase at 525 nm (YFP, acceptor) and a decrease at 474 nm (CFP, donor) indicative of FRET: YRC FRET occurred in the presence of Ran-GDP, whereas Ran-GTP induced maximal FRET of the YIC probe in the presence of importin  $\beta$ . To confirm the nucleotide dependence of the binding reactions biochemically, pull-down experiments were performed with purified proteins (Fig. 1C) (24). YRC bound Ran-GTP but not Ran-GDP. The interaction was fully reversible, because YRC that had bound to Ran-GTP could be released by the addition of Ran-GAP to induce Ran-GTP hydrolysis. Like full-length importin  $\alpha$ , YIC bound to importin  $\beta$  only in the absence of Ran-GTP.

**Fig. 1.** (A) Design of FRET probes. The YRC probe, consisting of a RBD fused to YFP and CFP, should undergo FRET in the presence of Ran-GDP but not when bound to Ran-GTP. The YIC probe consisting of the importin  $\beta$ -binding domain of importin  $\alpha$  (IBB) fused to YFP and CFP should undergo FRET when released from importin  $\beta$  by Ran-GTP. [(B) through (D)] Characterization of FRET probes with purified recombinant proteins. (B) Emission profiles showing the decrease in the CFP (donor) fluorescence peak at 474 nm and increase in the YFP (acceptor) fluorescence peak at 525 nm when FRET occurred. Reactions contained 0.2  $\mu$ M RCC1, 2  $\mu$ M Ran, and either 1 mM GDP (blue line) or 1 mM GTP (red line) with 1  $\mu$ M YRC (upper panel) or 1  $\mu$ M YIC plus 1.5  $\mu$ M importin  $\beta$  (lower panel). Samples were excited at 435 nm, and emission was measured from 460 to 550 nm at 0.5-nm increments. (C) Ran nucleotide state-dependent binding of probes can be detected biochemically. Ran-GTP but not Ran-GDP pulled down YRC, and this binding was abolished upon GTP hydrolysis induced by addition of Ran-GAP (upper panel). Importin  $\beta$  pulled down importin  $\alpha$  or YIC only in the absence of Ran-GTP (lower panel). (D) Reversibility of probe interactions. (Upper panel) FRET of YRC was diminished fractionally to a baseline level by addition of increasing amounts of Ran-GTP (arrowheads) but restored by subsequent addition of Ran-GAP causing GTP hydrolysis (arrow). (Lower panel) FRET of YIC was diminished by addition of importin  $\beta$  (arrow) but recovered upon addition of Ran-GTP (arrowheads). Experiments were performed with continuous stirring in a volume of 500  $\mu$ l. Samples were excited at 435 nm every 2 s, and emission at 474 nm ( $I_{CFP}$ ), 525 nm ( $I_{FRET}$ ), and the 525/474 ( $I_{FRET}/I_{CFP}$ ) ratio were obtained simultaneously.



Department of Molecular and Cell Biology, University of California, Berkeley, CA 94720–3200, USA.

\*To whom correspondence should be addressed. E-mail: heald@socrates.berkeley.edu (R.H.); kweis@uclink4.berkeley.edu (K.W.)

The fluorescent tags did not alter the affinity of the probe for importin  $\beta$  as compared to IBB or importin  $\alpha$  (25, 26). The rapid reversibility of FRET sensors was demonstrated by monitoring of emission intensity over time while the Ran nucleotide state was manipulated (Fig. 1D). The YRC FRET ratio calculated as the FRET emission at 535 nm upon excitation at 435 nm, divided by CFP emission at 474 nm ( $I_{\text{FRET}}/I_{\text{CFP}}$ ) decreased rapidly when its binding partner Ran-GTP was added and was restored upon addition of Ran-GAP. In contrast, the  $I_{\text{FRET}}/I_{\text{CFP}}$  ratio of YIC decreased quickly after the addition of importin  $\beta$  but was recovered upon Ran-GTP-induced release of the sensor.

Next we examined whether the FRET probes could also be used to monitor differences in the Ran nucleotide state in mitotic cytoplasmic extracts prepared from unfertilized *Xenopus* eggs (Fig. 2, A through C) (27, 28). Analogous to results with purified proteins (Fig. 1B), addition of a nonhydrolyzable Ran mutant loaded with GTP (Ran-Q69L-GTP) to extracts containing YRC caused a decrease in CFP donor emission and an increase in CFP acceptor emission, indicating a loss of YRC FRET (Fig. 2A), whereas YIC FRET in extract increased in the presence of Ran-Q69L-GTP (Fig. 2B). Similar results were obtained with the addition of RCC1, whereas addition of a large excess of Ran-GAP did not significantly alter FRET ratios

of YRC (Fig. 2C). Thus, at equilibrium, free Ran was predominantly in the GDP-bound form in cytoplasmic egg extracts.

As in solutions of pure proteins, FRET in the extract required both fluorophores to be on the same probe (29) and reflected specific binding reactions tightly regulated by Ran-GTP (Fig. 2D). Biotinylated sensors were retrieved from extracts by means of streptavidin beads (30). YRC did not bind endogenous Ran in untreated extracts but could capture exogenously added Ran-Q69L-GTP. Under these conditions, endogenous Ran also associated with YRC, indicating that addition of Ran-Q69L altered the Ran nucleotide state equilibrium in the extract to favor the GTP form. YIC was found associated with endogenous importin  $\beta$  in extracts, but this interaction was lost upon addition of Ran-Q69L-GTP. Thus, our FRET probes detected dynamic changes in the Ran nucleotide state and importin  $\beta$ -cargo binding in egg extracts and indicate that endogenous Ran in egg extracts is predominantly in its GDP-bound form.

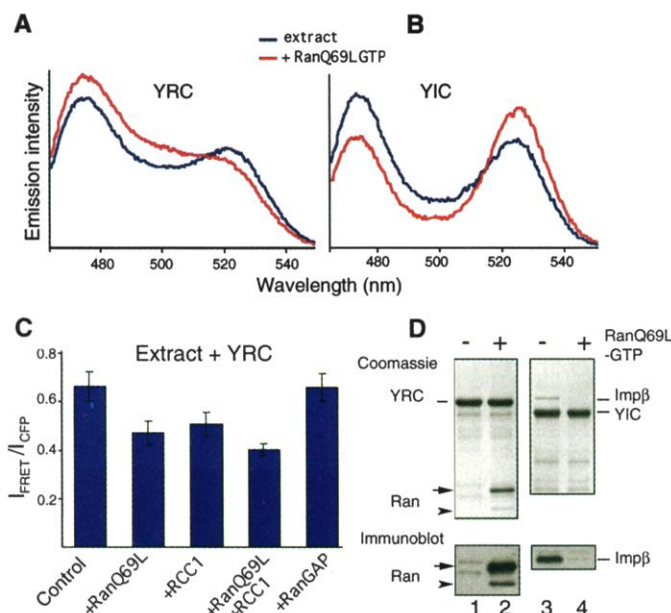
To test whether our sensors could allow visualization of a Ran-GTP gradient generated by chromosome-bound RCC1 during mitosis, *Xenopus* sperm nuclei were added to mitotic egg extracts supplemented with FRET probes and rhodamine-labeled tubulin (Fig. 3A). Spindle assembly and FRET were both monitored by fluorescence microscopy

(31). After 30 min of incubation, spindle assembly was apparent, as rhodamine-labeled tubulin incorporated into bipolar structures with chromosomes positioned at the metaphase plate. Visualization of the YRC probe revealed a gain in CFP fluorescence intensity ( $I_{\text{CFP}}$ ) and a relative decrease in FRET emission intensity ( $I_{\text{FRET}}$ ) in the immediate vicinity of the chromosomes. As a result, the  $I_{\text{FRET}}/I_{\text{CFP}}$  ratio of the YRC probe was the lowest in the central spindle, indicating localized loss of YRC intramolecular FRET due to its binding to Ran-GTP generated by chromosome-bound RCC1. Conversely, the YIC probe exhibited a decreased  $I_{\text{CFP}}$  signal and an increased  $I_{\text{FRET}}$  signal in the region surrounding the chromosomes of the spindle. The high FRET ratio ( $I_{\text{FRET}}/I_{\text{CFP}}$ ) levels in the central spindle thus revealed a gradient of YIC liberated from importin  $\beta$ , indicating localized release of cargoes by Ran-GTP. Results obtained with  $I_{\text{FRET}}/I_{\text{CFP}}$  ratio imaging were supported by FRET images normalized for probe concentration and channel cross-bleed (32, 33) that displayed YRC and YIC FRET gradients of similar proportions and steepness (29). When probes were substituted with a mixture of individually labeled RBD-YFP and RBD-CFP or IBB-YFP and IBB-CFP constructs or with a sensor unresponsive to the Ran nucleotide state, no FRET signal was detectable, demonstrating that the changes were specific and caused by intramolecular FRET (29).

The establishment of Ran-GTP and liberated cargo gradients preceded microtubule polymerization into polarized arrays, because YRC and YIC  $I_{\text{FRET}}/I_{\text{CFP}}$  ratio gradients were visible around sperm nuclei within several minutes after the initiation of spindle assembly reactions (29).

If chromatin-bound RCC1 is responsible for formation of the mitotic Ran-GTP gradient and the downstream gradient of released cargoes, then inhibition of RCC1 function should disrupt localized FRET of both the YRC and YIC probes. Furthermore, if these gradients are physiologically meaningful, their disruption should affect spindle assembly. Addition of Ran-T24N, a potent inhibitor of RCC1, eliminated FRET ratio gradients of both probes and caused a decrease in microtubule density in spindles (Fig. 3B). In contrast, addition of nonhydrolyzable Ran-Q69L-GTP led to spontaneous microtubule polymerization and formation of spindle-like structures independent of chromosomes (4–8). Under these conditions, fluorescence microscopy revealed uniform  $I_{\text{FRET}}/I_{\text{CFP}}$  signals without a gradient surrounding chromosomes, with overall lower YRC and elevated YIC  $I_{\text{FRET}}/I_{\text{CFP}}$  ratios consistent with results obtained by fluorimetry in the presence of Ran-Q69L-GTP (Fig. 2, A through C). In contrast, addition of the Ran-GTP-indepen-

**Fig. 2.** Characterization of FRET probes in *Xenopus* egg extracts. (A and B) Emission profiles showing a decrease in the CFP donor fluorescence peak at 474 nm and an increase in the acceptor fluorescence peak at 525 nm when FRET occurred. (A) FRET of 2  $\mu\text{M}$  YRC in extract (blue line) was decreased upon addition of 30  $\mu\text{M}$  Ran-Q69L-GTP (red line). (B) FRET of YIC in extract (blue line) was increased upon Ran-Q69L-GTP addition (red line). Samples were excited at 435 nm, and emission was measured from 465 to 550 nm at 0.5-nm increments. (C) Free Ran in the extract was predominantly in the GDP-bound form. The FRET ratio of the YRC probe was diminished by the addition of 50  $\mu\text{M}$  Ran-Q69L or 5  $\mu\text{M}$  RCC1 that increased the concentration of Ran-GTP but was unaffected by the addition of 6  $\mu\text{M}$  Ran-GAP. Data represent the average of at least four experiments. (D) Probe interactions in extracts detected biochemically. No detectable Ran was pulled down with YRC from untreated extracts (lane 1), whereas exogenously added Ran-Q69L-GTP was retrieved (arrow) along with some endogenous Ran (arrowhead), as confirmed by immunoblot with antibody to Ran (lane 2). YIC retrieved endogenous importin  $\beta$  from untreated extracts (lane 3), as confirmed by immunoblot with antibody to importin  $\beta$ , but this interaction was blocked by the addition of Ran-Q69L-GTP (lane 4).



dent cargo-binding domain of importin  $\beta$  (amino acids 71 through 876) eliminated the  $I_{\text{FRET}}/I_{\text{CFP}}$  ratio signal displayed by the YIC

probe by interfering with the release of this cargo, but did not disrupt the Ran-GTP gradient visualized directly with the YRC sen-

sor. Thus, importin  $\beta$  cargo release functions downstream of the Ran-GTP gradient, and, consistent with previous data, sequestering of importin  $\beta$  cargoes caused defects in microtubule polymerization and organization (11).

Next we used the YRC probe to analyze the distribution of the Ran nucleotide state in nuclei formed in interphase egg extracts (Fig. 3C). Although the YRC probe was enriched in the nucleus, specific loss of  $I_{\text{FRET}}/I_{\text{CFP}}$  was observed in this compartment, revealing a very high enrichment of Ran in its GTP-bound form in the nucleoplasm. An increase in YRC FRET in the nucleus was observed upon addition of either the RCC1 inhibitor Ran-T24N or the Ran-GTP binding domain of importin  $\beta$  (Fig. 3C) (29). Based on the Ran-GTP occupancy of the YRC sensor and its affinity for Ran-GTP, we estimated that the concentration difference between free nuclear and cytoplasmic Ran-GTP was at least 200-fold.

The FRET probes reported here enable highly sensitive monitoring of spatial and temporal changes in both the Ran nucleotide state and importin  $\beta$ -cargo interactions throughout the cell cycle. This analysis reveals that mitotic chromosomes are surrounded by a Ran-GTP gradient that induces a gradient of liberated cargoes and that a steep Ran-GTP concentration difference exists between the nucleus and cytoplasm during interphase. Our observations provide direct evidence that a chromatin-generated Ran-GTP gradient is maintained throughout the cell cycle and support the model that Ran-GTP acts as a positional marker of the genome.

References and Notes

1. M. Dasso, *Cell* **104**, 321 (2001).
2. I. W. Mattaj, L. Englmeier, *Annu. Rev. Biochem.* **67**, 265 (1998).
3. D. Görlich, U. Kutay, *Annu. Rev. Cell Dev. Biol.* **15**, 607 (1999).
4. P. Kalab, R. T. Pu, M. Dasso, *Curr. Biol.* **9**, 481 (1999).
5. R. E. Carazo-Salas *et al.*, *Nature* **400**, 178 (1999).
6. T. Ohba, M. Nakamura, H. Nishitani, T. Nishimoto, *Science* **284**, 1356 (1999).
7. A. Wilde, Y. Zheng, *Science* **284**, 1359 (1999).
8. C. Zhang, M. Hughes, P. R. Clarke, *J. Cell Sci.* **112**, 2453 (1999).
9. M. Hetzer, D. Bilbao-Cortes, T. C. Walther, O. J. Gruss, I. W. Mattaj, *Mol. Cell* **5**, 1013 (2000).
10. C. Zhang, P. R. Clarke, *Science* **288**, 1429 (2000).
11. M. V. Nachury *et al.*, *Cell* **104**, 95 (2001).
12. O. J. Gruss *et al.*, *Cell* **104**, 83 (2001).
13. C. Wiese *et al.*, *Science* **291**, 653 (2001).
14. The RBD-encoding region of *Saccharomyces cerevisiae* Yrb1 (RBD, corresponding to amino acids 37 through 201), the importin  $\beta$ -binding domain of importin  $\beta$  (IBB, corresponding to amino acids 1 through 65), and CFP and YFP (Clontech) were amplified by polymerase chain reaction and/or subcloned to generate 6XHis tagged YRC (pKW 966), RY (pKW 985), RC (pKW 984), YIC (pKW 970), IY (pKW 960), and IC (pKW 958) expression constructs in pRSET (Invitrogen) that were verified by sequencing. All YFP and CFP fusion proteins were expressed in bacterial strain BL21 DE3 at room temperature.
15. R. Y. Tsién, A. Miyawaki, *Science* **280**, 1954 (1998).
16. G. Schlenstedt, D. H. Wong, D. M. Koepf, P. A. Silver, *EMBO J.* **14**, 5367 (1995).
17. I. R. Vetter, C. Nowak, T. Nishimoto, J. Kuhlmann, A. Wittinghofer, *Nature* **398**, 39 (1999).

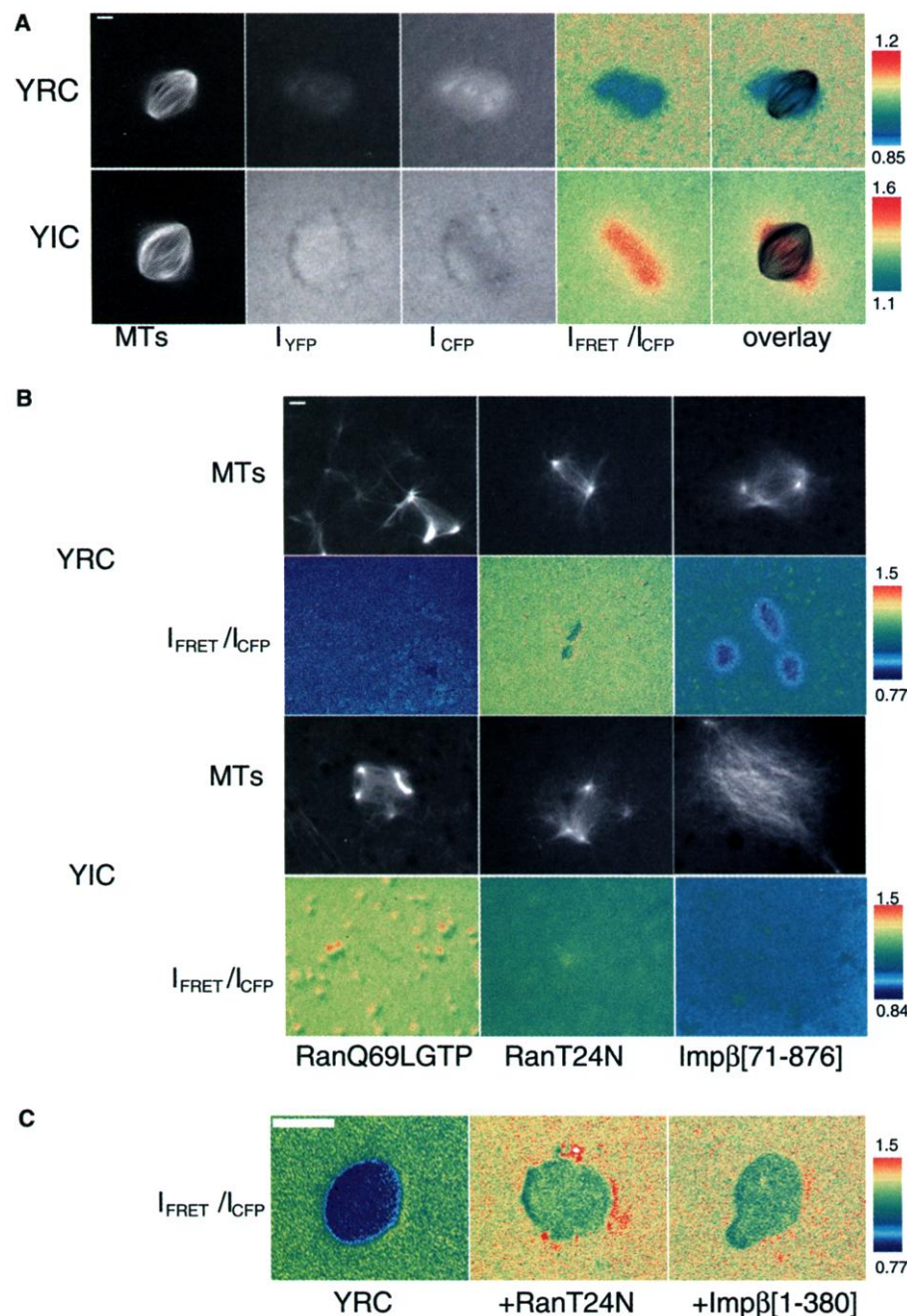


**Fig. 3.** A gradient of Ran-GTP surrounding chromosomes visualized in egg extracts and abolished by the addition of Ran mutants. Scale bars, 10  $\mu\text{m}$ . (A) Fluorescence images of mitotic spindles showing microtubules (MTs) and  $I_{\text{YFP}}$ ,  $I_{\text{CFP}}$ , and FRET ratio ( $I_{\text{FRET}}/I_{\text{CFP}}$ ) signals, and an MT-FRET ratio overlay showing a decrease in FRET surrounding chromosomes in the presence of YRC and an increase in the presence of YIC due to the presence of Ran-GTP. There is a decrease in  $I_{\text{CFP}}$  in regions where FRET occurs. (B) Addition of 30  $\mu\text{M}$  exogenous Ran-Q69L-GTP caused a loss of localized YRC and YIC FRET ratio signals and distortion of spindle structures due to ectopic microtubule polymerization. Addition of 30  $\mu\text{M}$  Ran-T24N inhibited RCC1, abolished localized FRET ratio gradients around chromosomes as detected by both probes, and destabilized spindle microtubules. Addition of the cargo-binding domain of importin  $\beta$  [Imp $\beta$ (71-876), 10  $\mu\text{M}$ ] did not distort the Ran-GTP gradient visualized with YRC but sequestered importin  $\beta$  cargoes, including YIC, uniformly abolishing its FRET signal and demonstrating that proper cargo release was required to maintain spindle morphology. (C) The Ran-GTP gradient in interphase visualized with the YRC probe. Addition of 30  $\mu\text{M}$  RCC1 inhibitor Ran-T24N or 30  $\mu\text{M}$  importin  $\beta$  Ran-GTP binding domain [Imp $\beta$ (1-380)] diminished nuclear Ran-GTP.

18. M. Rexach, G. Blobel, *Cell* **83**, 683 (1995).
19. D. Görlich, P. Henklein, R. A. Laskey, E. Hartmann, *EMBO J.* **15**, 1810 (1996).
20. K. Weis, C. Dingwall, A. I. Lamond, *EMBO J.* **15**, 7120 (1996).
21. B. Kobe, *Nature Struct. Biol.* **6**, 388 (1999).
22. G. Cingolani, C. Petosa, K. Weis, C. W. Müller, *Nature* **399**, 221 (1999).
23. Emission spectra were analyzed with a Fluorolog 2 spectrophotometer controlled by Datamax 2.2 (Jobin Yvon Spex) and the Grams 3.04 II software package (Galactic Industries, Salem, NH). Both excitation and emission slits were set at 2 nm and voltage at 950 V.
24. Recombinant S-tagged Ran (2  $\mu$ M) preloaded with either GTP or GDP was incubated with 4  $\mu$ M purified YRC in phosphate-buffered saline on ice for 30 min. The Ran-GTP reaction was split into two aliquots, and one sample was treated with 100 ng of recombinant Ran-GAP. S-tagged importin  $\beta$  (2  $\mu$ M) was incubated with recombinant importin  $\alpha$  or YIC (each at 2  $\mu$ M final concentration) in either the presence or absence of Ran preloaded with GTP (4  $\mu$ M). Proteins bound to Ran or importin  $\beta$  were retrieved on protein-S-agarose beads, eluted with sample buffer, and analyzed by SDS-polyacrylamide gel electrophoresis (SDS-PAGE).
25. Dissociation constants between the YIC sensor, IBB, or importin  $\alpha$  and  $\beta$  were measured with the Ran-GAP protection assay (34) (P. Kalab, K. Weis, R. Heald, unpublished data).
26. B. Catimel et al., *J. Biol. Chem.* **276**, 34189 (2001).
27. Cytostatic factor (CSF)-arrested extracts of *Xenopus* eggs were supplemented with 500 demembrated *Xenopus* sperm nuclei/ $\mu$ l and X-rhodamine-labeled tubulin (0.1 mg/ml) to visualize microtubules. Entry into interphase was induced by the addition of 0.4 mM CaCl<sub>2</sub>. If not indicated otherwise, 2  $\mu$ M YRC or YIC probe was added. Both excitation and emission slits were set at 15 nm and voltage at 550 V.
28. A. W. Murray, *Methods Cell Biol.* **36**, 581 (1991).
29. Supplementary material is available on Science Online at [www.sciencemag.org/cgi/content/full/295/5594/2452/DC1](http://www.sciencemag.org/cgi/content/full/295/5594/2452/DC1).
30. For pull-downs from extract with streptavidin beads, YIC and YRC were biotinylated with dithiothreitol (DTT)-cleavable biotinylation reagent (EZ-Link Sulfo-NHS-ss-Biotin, Pierce, no. 21331) according to the manufacturer's instructions in a 5:1 molar biotin excess, and dialyzed against XB. Biotinylation did not inhibit probe FRET or affect in vitro binding interactions (P. Kalab, K. Weis, R. Heald, data not shown). Streptavidin beads (Pierce, no. 53117) were combined with biotinylated probes on ice for 20 min, washed with extract buffer (XB) (28), and mixed with 50  $\mu$ l of CSF extract supplemented with either 30  $\mu$ M Ran-Q69L-GTP or an equal volume of XB. After incubation at room temperature for 20 min, beads were pelleted and washed extensively, and bound proteins were eluted with 100 mM DTT and analyzed by SDS-PAGE and immunoblot with antibodies specific for Ran and importin  $\beta$ .
31. Images were collected with a  $\times 40$  Plan Fluor lens (Nikon) and a  $\times 10$  CFI objective using a Nikon E600 fluorescent microscope equipped with a cooled Hamamatsu charge-coupled device camera (C4742-98), Lambda 10-2 (Sutter) shutter controller, and a manual sliding filter cube holder (Nikon). The filter set for YFP emission fluorescence ( $I_{YFP}$ ) consisted of exciter HQ500/20, dichroic Q515LP, and emitter HQ535/30. The CFP fluorescence ( $I_{CFP}$ ) was collected with exciter D436/20, dichroic 455DCLP, and emitter D480/40. The CFP/YFP energy transfer emission ( $I_{FRET}$ ) was imaged with exciter D436/20, dichroic 455DCLP, and emitter D535/30. X-rhodamine-labeled tubulin was visualized with an HQ-TRITC filter cube. All filters sets were made by Chroma. Images were acquired consecutively by TRITC (0.2 to 0.5 s) followed by YFP, CFP, and FRET cubes (with an identical setting within each sample, 1 or 2 s each) using Metamorph 4.6 imaging software (Universal Imaging) with no binning.  $I_{FRET}/I_{CFP}$  ratio images were calculated from 14-bit  $I_{FRET}$  and  $I_{CFP}$  images by Metamorph "Ratio" function and displayed in pseudocolor within the ratio range 0.7 to 1.3 for YRC samples and in the range 0.7 to 1.8 for YIC-containing samples.

Images in 14 bits were converted to 8 bits with NIH Image 1.6, and all images were composed with Adobe Photoshop 5.5.

32. Z. Xia, Y. Liu, *Biophys. J.* **81**, 2395 (2001).
33. G. W. Gordon, G. Berry, X. H. Liang, B. Levine, B. Herman, *Biophys. J.* **74**, 2702 (1998).
34. We thank A. Dernburg and members of the Heald and Weis labs for helpful discussions and/or comments

on the manuscript, M. Welch for help with fluorimetry, Y. Azuma for help with RCC1 purification, M. Ignatius for help with microscopy, and G. O. Nads for sperm nuclei. Funded by grants from NIH and the Pew Scholars Program (R.H.) and the Searle Scholars Program (K.W.).

7 December 2001; accepted 25 February 2002

## Systemic RNAi in *C. elegans* Requires the Putative Transmembrane Protein SID-1

William M. Winston, Christina Molodowitch, Craig P. Hunter\*

Double-stranded RNA-mediated gene interference (RNAi) in *Caenorhabditis elegans* systemically inhibits gene expression throughout the organism. To investigate how gene-specific silencing information is transmitted between cells, we constructed a strain that permits visualization of systemic RNAi. We used this strain to identify systemic RNA interference-deficient (*sid*) loci required to spread gene-silencing information between tissues but not to initiate or maintain an RNAi response. One of these loci, *sid-1*, encodes a conserved protein with predicted transmembrane domains. SID-1 is expressed in cells sensitive to RNAi, is localized to the cell periphery, and is required cell-autonomously for systemic RNAi.

One of the first reported and still mysterious aspects of RNAi in *C. elegans* is that it is systemic. Injection of gene-specific double-stranded RNA (dsRNA) into one tissue leads to the posttranscriptional silencing of that gene in other tissues and in that worm's progeny (1). The systemic nature of RNAi also provides for initiation of RNAi by soaking animals in dsRNA (2, 3) or by cultivating worms on bacteria expressing dsRNA (4, 5). Although systemic RNAi has not been demonstrated in any other animal, systemic posttranscriptional gene silencing (PTGS) effects in plants are well established (6, 7). PTGS appears to play a role in viral defense (8); at the same time, viruses are able to inhibit systemic PTGS (9).

Genes required for RNAi have been identified in a variety of systems, as have small interfering RNAs (siRNAs) that can directly trigger RNAi and act as guide RNAs that direct sequence-specific mRNA cleavage (10–12). Among the *C. elegans* genes required for RNAi are *rde-1* and *rde-4*, which have no readily detectable mutant phenotype other than resistance to RNAi (13). These mutants are resistant to dsRNA targeting both somatic and germ line-specific genes and are also resistant to dsRNA produced by transgenes (13). However, these genes are not involved in systemic RNAi, because ho-

mozygous *rde-1* or *rde-4* mutant animals injected in the intestine with dsRNA are capable of efficiently transporting the RNAi effect to heterozygous cross progeny (13). It is noteworthy that *rde-4* is required for the efficient production of siRNAs (14), suggesting that siRNAs are not required for systemic RNAi.

To specifically investigate systemic RNAi, we constructed a transgenic strain (HC57) that allows simultaneous monitoring of localized and systemic RNAi. HC57 expresses two green fluorescent protein (GFP) transgenes, one expressed in the pharyngeal muscles (*myo-2::GFP*) and the other expressed in the body-wall muscles (*myo-3::GFP*). To initiate RNAi, a third transgene was introduced that expresses a GFP dsRNA construct under the control of the pharynx-specific *myo-2* promoter (*myo-2::GFP dsRNA*) (15). In HC57, localized RNAi of *myo-2::GFP* in the pharynx was highly penetrant, but incomplete and temperature sensitive (Fig. 1B, compare with 1A), whereas systemic RNAi of *myo-3::GFP* in body-wall muscle was position-dependent and also temperature-sensitive (Fig. 1, B and C) (15). Systemic RNAi did not require expression of GFP in the pharynx, as expression of only *myo-2::GFP dsRNA* led to silencing of GFP in body-wall muscle (Fig. 1D). Silencing in both the pharynx and body-wall muscles was dependent on *rde-1*, verifying that the silencing was due to RNAi (Fig. 1G).

We used the HC57 strain to identify systemic RNA interference defective (*sid*) mutants, by screening for animals resistant to systemic RNAi of *myo-3::GFP* in the body-

Department of Molecular and Cellular Biology, Harvard University, 16 Divinity Avenue, Cambridge, MA 02138, USA.

\*To whom correspondence should be addressed. E-mail: [hunter@mcb.harvard.edu](mailto:hunter@mcb.harvard.edu)